

The Effect of the Substituent Length in Protic Ionic Liquid Additive on the Corrosion Process in the Lead–Acid Battery

Kacper Kopczyński¹, Agnieszka Gabryelczyk¹, Marek Baraniak¹, Bartosz Łęgosz¹, Juliusz Pernak¹, Paweł Kędzior², Grzegorz Lota^{1,*}

¹ Faculty of Chemical Technology, Poznan University of Technology, Berdychowo 4, 60–965 Poznan, Poland

² PPUH AUTOPART Jacek Bąk Sp. z o.o., Kwiatkowskiego 2a, 39–300 Mielec, Poland

* E-mail: grzegorz.lota@put.poznan.pl

Received: 8 January 2018 / Accepted: 7 March 2018 / Published: 10 April 2018

Modern automotive industry still relies on the lead-acid batteries as a power supply for starting, lighting and ignition applications. In order to provide efficient devices, manufacturers should control the quality and electrochemical properties of the product. One of the disadvantages of the lead–acid batteries is the corrosion process of the current collectors in the lead–acid batteries. In the presented work, an investigation of the influence of the protic ionic liquids on the corrosion process and gas evolution in the lead alloy/sulfuric acid electrochemical system has been conducted. The aim was to correlate the substituent length in the ionic liquid cation with the electrochemical window of the modified electrolytes and corrosion behavior of the lead alloy. Five new compounds were synthesized and their properties as ionic liquids were confirmed using thermogravimetric analysis and differential scanning calorimetry. The techniques used during the electrochemical experiments include linear sweep voltammetry and electrochemical impedance spectroscopy. The obtained results revealed that the electrochemical stability of the electrolytes increases with the length of the substituent. Satisfactory change was observed also in the corrosion behavior of the modified systems.

Keywords: Corrosion; hydrogen evolution; side–chain length; current collector; lead–acid battery

1. INTRODUCTION

Adequate maintenance is a key aspect for the long service life of lead–acid cells. However, even the most carefully operated battery undergoes some internal changes, which lead to the reduction of the device parameters such as current efficiency, capacity, and conductivity of the active mass or current collectors. One of the most common reasons for the above-mentioned phenomena is corrosion of the current collectors in lead–acid battery (LAB) [1,2]. Current collector, called the grid in LAB,

also acts as support for the active material. Initially, corrosion occurs during the curing process of the plates, which results in enhanced adhesion of active paste to the surface of the grid [3]. At that stage, the processes of the lead alloy oxidation enable both components to constitute and retain a proper mechanical contact, hence, initial corrosion has beneficial influence on the materials and is necessary in terms of the battery construction and efficient operation. Afterwards, the corrosion process takes place during charging, when the positive electrode is oxidised due to applied high potentials. Corrosion products formed on the surface of the current collectors are incorporated into the active mass as impurities, changing its electrochemical properties. Thus, corrosion influences the adhesive properties of materials and contributes to the shedding of active mass. Therefore, premature capacity loss can occur. The negative current collector is notably less affected by corrosion [4]. However, under certain conditions hydrogen corrosion and faster self-discharge can be observed due to the enhanced hydrogen evolution [5,6].

According to the thermodynamic point of view, corrosion of a material is a spontaneous and inevitable process of transition to its more stable form in the current environment. However, several means of controlling the corrosion rate are known, namely, changes in the operating conditions of the system (e.g. temperature, ions concentration), alloying additives (providing corrosion inhibition to the alloys), and modification of the electrolyte composition [7]. The last-mentioned method is carried out by dissolving small amounts of selected substances in the electrolyte, therefore, implementation of this method in the laboratory and industrial practice is simple and economically justified. This modification includes additions of compounds such as boric acid and borates, phosphoric acid and phosphates, thiourea and its derivatives, or surfactants [8–11]. Modern chemistry supplied a novel and promising group of organic compounds called ionic liquids (ILs) to be investigated in the field of materials science. Beneficial influence of these compounds on corrosion inhibition has been reported by various researchers not only in case of metal constructions [12,13] but secondary cells as well [7,14–16]. The decrease of corrosion intensity can also be observed in lead–acid batteries [17,18]. It has been confirmed that certain representatives of ionic liquids have a significant influence on the hydrogen evolution reaction, changing the potential of the process, so that less gaseous products are generated during battery operation [6,19]. The other advantage of this property is the broadening of the electrochemical window of the electrolyte, which can contribute to increased operating voltage of the cell. Moreover, ionic liquids have been used as electrolytes for supercapacitors and lithium–ion batteries [20] and as binders for electroactive materials [21]. This particular abundance of the properties applicable in electrochemistry is owed to characteristics of ionic liquids as designer compounds, which enables synthesising compounds featured by high thermal and electrochemical stability, low vapour pressure and good ionic conductivity [22–24].

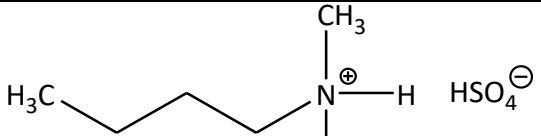

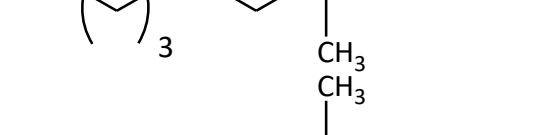
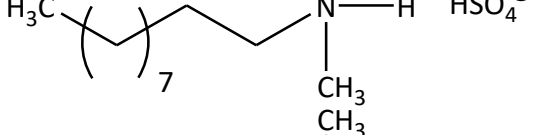
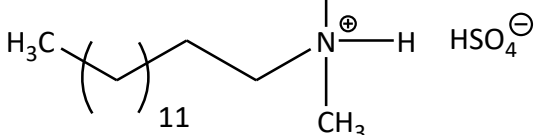
In this paper, the influence of the side chain length in the protic quaternary ammonium ionic liquids on the electrochemical properties of $\text{PbCaSn|H}_2\text{SO}_4$ has been investigated. Five ionic liquids have been used to modify the standard lead–acid battery electrolyte (37 wt.% sulfuric acid solution). The pursued assignments of the study include the investigation of the electrochemical window of electrolytes as well as the corrosion inhibition measurements of the lead–calcium–tin alloy.

2. EXPERIMENTAL

2.1. Synthesis of ionic liquids

Substrates for the synthesis of five quaternary ammonium ionic liquids with bisulfate anion: N,N-dimethylbutylamine (99%), N,N-dimethylhexylamine (98%), N,N-dimethyloctylamine (95%), N,N-dimethyldecylamine (98%), N,N-dimethyltetradecylamine ($\geq 95\%$), N,N-dimethylhexadecylamine ($\geq 95\%$) and sulfuric acid (98%) were purchased from Merck and hexane ($\geq 95\%$) was delivered by Avantor Performance Materials. The above-mentioned compounds were used without further purification. To carry out the process, 0.01 mol of respective amine was dissolved in 50 mL of hexane. The solution was stirred vigorously while 0.01 mol of concentrated sulfuric acid was slowly added. The product precipitated from the solution as a white solid. After 15 minutes the mixture was cooled down to ambient temperature and then the precipitate was separated from the solvent using vacuum filtration. The obtained product was dried at 60°C under reduced pressure. The structural formulas of the protic ionic liquids are presented below (Table 1).

Table 1. Chemical formulas and names of the compounds used in the study with abbreviations distinguishing the length of carbon side chain in the molecule

No.	Chemical name	Structural formula	Abbreviation
1	Dimethylbutylammonium bisulfate		HC4
2	Dimethylhexylammonium bisulfate		HC6
3	Decyldimethylammonium bisulfate		HC10
4	Dimethyltetradecylammonium bisulfate		HC14
5	Dimethylhexadecylammonium bisulfate		HC16

2.2. Elemental analysis and NMR spectroscopy of ionic liquids

^1H NMR and ^{13}C NMR spectra were recorded using Varian Mercury 300 spectrometer operating at 300 MHz with TMS as the internal standard and at 75 MHz, respectively.

Dimethylbutylammonium bisulfate (HC4): ^1H NMR (300 MHz, CDCl_3): 0.88–0.92 (t, 3H); 1.30–1.33 (m, 2H); 1.69–1.73 (m, 2H); 2.99 (s, 6H); 3.06–3.12 (m, 2H).

^{13}C NMR (75 Hz, CDCl_3): 14.1; 23.5; 25.4; 27.3; 32.3; 43.5; 59.1.

Elemental analysis: CHN for $\text{C}_6\text{H}_{17}\text{NO}_4\text{S}$ ($M = 199.27 \text{ g mol}^{-1}$): calcd.: C = 36.16; H = 8.60; N = 7.03; found: C = 36.50; H = 8.92; N = 6.88.

Dimethylhexylammonium bisulfate (HC6): ^1H NMR (300 MHz, CDCl_3): 0.90–0.94 (t, 3H); 1.34–1.39 (m, 6H); 1.72–1.76 (m, 2H); 2.89 (s, 6H); 3.10–3.14 (m, 2H).

^{13}C NMR (75 Hz, CDCl_3): 14.3; 23.5; 25.6; 27.1; 32.4; 43.5; 59.0.

Elemental analysis: CHN for $\text{C}_8\text{H}_{21}\text{NO}_4\text{S}$ ($M = 227.32 \text{ g mol}^{-1}$): calcd.: C = 42.27; H = 9.31; N = 6.16; found: C = 42.58; H = 9.63; N = 5.88.

Decyldimethylammonium bisulfate (HC10): ^1H NMR (300 MHz, CDCl_3): 0.87–0.92 (t, 3H); 1.30–1.37 (m, 14H); 1.73–1.75 (m, 2H); 2.88 (s, 6H); 3.08–3.13 (m, 2H).

^{13}C NMR (75 Hz, CDCl_3): 14.5; 23.7; 25.6; 27.5; 30.3; 30.4; 30.5; 30.6; 33.0; 43.5; 59.0.

Elemental analysis: CHN for $\text{C}_{12}\text{H}_{29}\text{NO}_4\text{S}$ ($M = 283.43 \text{ g mol}^{-1}$): calcd.: C = 50.85; H = 10.31; N = 4.94; found: C = 51.07; H = 10.66; N = 4.61.

Dimethyltetradecylammonium bisulfate (HC14): ^1H NMR (300 MHz, CDCl_3): 0.89–0.93 (t, 3H); 1.21–1.25 (m, 22H); 1.66–1.71 (m, 2H); 2.93 (s, 6H); 3.07–3.14 (m, 2H).

^{13}C NMR (75 Hz, CDCl_3): 14.3; 23.6; 25.7; 27.5; 30.2; 30.4; 30.5; 30.6; 32.9; 43.6; 59.2.

Elemental analysis: CHN for $\text{C}_{16}\text{H}_{37}\text{NO}_4\text{S}$ ($M = 339.53 \text{ g mol}^{-1}$): calcd.: C = 56.60; H = 10.98; N = 4.13; found: C = 56.73; H = 11.23; N = 3.95.

Dimethylhexadecylammonium bisulfate (HC16): ^1H NMR (300 MHz, CDCl_3): 0.87–0.92 (t, 3H); 1.22–1.37 (m, 26H); 1.68–1.78 (m, 2H); 2.88 (s, 6H); 3.08–3.14 (m, 2H).

^{13}C NMR (75 Hz, CDCl_3): 14.5; 23.8; 25.7; 27.5; 30.3; 30.5; 30.6; 30.7; 30.8; 30.9; 33.1.

Elemental analysis: CHN for $\text{C}_{18}\text{H}_{41}\text{NO}_4\text{S}$ ($M = 367.59 \text{ g mol}^{-1}$): calcd.: C = 58.81; H = 11.24; N = 3.81; found: C = 59.07; H = 11.59; N = 3.56.

2.3. Thermal analysis of ionic liquids

Temperatures of the thermal transition were determined by differential scanning calorimetry (DSC) with a Mettler Toledo Star DSC1 unit (Leicester, UK) under nitrogen atmosphere. A sample of every respective ionic liquid (the amount between 5 and 15 mg) was placed in an aluminium pan and heated from 25 to 120 °C at a heating rate of 10 °C min⁻¹, then cooled with an intracooler to -100 °C at a cooling rate of 10 °C min⁻¹, and heated again to 120 °C afterwards. Thermogravimetric analysis was performed using Mettler Toledo Stare TGA/DSC1 (Leicester, UK) under nitrogen atmosphere. ILs (between 2 and 10 mg) were placed in aluminium pans and heated from 30 to 450 °C at a heating rate of 10 °C min⁻¹.

2.4. Electrochemical measurements

Electrochemical measurements were carried out in the 3-electrode configuration in the cylindrical vessel with the lead-calcium-tin alloy as a working electrode, pure lead as a counter electrode and mercury/mercurous sulfate reference electrode ($\text{Hg}|\text{Hg}_2\text{SO}_4$ in 1M H_2SO_4). Vents were located in the top lid of the above-mentioned vessel in order to release gaseous products from the container. Lead alloy and pure lead were delivered by AutoPart company (Mielec, Poland) in the form of wide straps of material prepared for further processing (expanded metal method). The working electrode was shaped into a circle with the surface area equal to 4.5 cm^2 . The surface area of the counter electrode was two times greater to provide effective charge transfer in the circuit. Before the experiment, the surface of the working and counter electrodes were prepared by mechanical polishing with wet sandpaper (grade P2500). The improvement of modelling and the accuracy of the $\text{Pb}|\text{H}_2\text{SO}_4$ system prepared for the study was achieved by using the industrial-grade alloy for the positive current collector in lead-acid battery and the adequate concentration of the electrolyte as well. The electrolyte was 37 wt.% sulfuric acid solution prepared by dissolution of the appropriate amount of pure substance (98%, Merck) in distilled water. The obtained liquid solution was employed as a reference electrolyte for the electrochemical experiments in order to distinguish the initial corrosion parameters of PbCaSn alloy and thus, the influence of the organic additive. Modification of the reference electrolyte was conducted by adding the previously obtained ionic liquids to the solution. Thus, five modified environments were created, each containing 5 mg cm^{-3} of the respective ionic liquid. The specific amount of the additive was dictated by the results of previously carried out experiments, which stated that the amount lower than that which was applied gives unsatisfactory values of conductivity. On the other hand, a higher amount leads to strong effect of the electrolyte foaming, which is a disadvantage in terms of the overall performance of the electrochemical system and the battery.

Experiments performed using linear sweep voltammetry and impedance spectroscopy allowed to specify properties such as electrochemical stability of the electrolytes (potential window) and corrosion parameters of the working electrode in the modified environment (corrosion current density and potential, polarization resistance). The electrochemical stability of the electrolyte was measured by linear sweep voltammetry (LSV) at a scan rate of 10 mV s^{-1} . Corrosion behavior of the lead alloy in the six electrolytes was analyzed using LSV at a scan rate of 0.2 mV s^{-1} and within a potential range of $\pm 180 \text{ mV}$ versus open circuit potential (OCP). Polarization resistance was evaluated based on the data obtained by electrochemical impedance spectroscopy (EIS) within the frequency range from 50 mHz to 10 kHz, overall number of points equal to 200 and sinus amplitude V_{rms} at $\pm 7 \text{ mV}$.

Experiments were performed under ambient conditions using the multichannel potentiostat/galvanostat VMP3 BioLogic® (France) with EC-Lab® software and repeated at least three times. The numbers presented in the table are average values of calculated parameters.

3. RESULTS AND DISCUSSION

3.1 Structure and thermal stability of ionic liquids

The structures of the synthesized products were confirmed by analysis of NMR spectra. Protons from alkyl substituents were recorded as signals in the range from 0.87 to 0.94 for methyl groups. Protons in methylene groups were identified as peaks between 1.22 and 1.39 ppm. Methylene groups in position β to quaternary nitrogen atom occurred as signals from 1.68 to 1.78 ppm, while protons in position α were noted in range the from 3.08 to 3.14 ppm. Two methyl groups were identified as high peaks at 2.88–2.89 ppm.

The synthesized compounds can be classified as ionic liquids – their melting temperatures were noted below 100°C. The phase transitions and their characteristic temperatures are determined by the length of alkyl substituents (Table 2). No phase transitions were noted for HC4 in the temperature range from –100 to 120°C. Elongation of substituents resulted in the occurrence of glass transition temperature at –69°C for HC6. No crystallization or melting was observed. For ILs with moderate length of substituents (HC10) all phase transitions were observed. For HC10 transitions were noted at –59°C, –38°C and –10°C, respectively. Further elongation of substituent reversed this trend. No glass transition was noted for salts with the longest alkyl chains (HC14, HC16). Few steps of crystallization and melting were observed. For HC14 the temperatures of crystallization were noted at 1°C, 40°C and 50°C and melting at 0°C, 40°C, and 65°C. Slightly higher values were measured for HC16 – crystallization at 13°C and 61°C and melting at 10°C, 46°C, 64°C. The multiple crystallization and melting steps can be explained by transitions between amorphous forms of the compound. The influence of the alkyl substituent length on values of phase transition temperatures was also noted for other quaternary ammonium salts [25].

Table 2. Transition temperatures of the synthesized compounds

IL	T _g	T _c	T _m (°C)	T _{onset5%}	T _{onset50%}
HC4	–	–	–	260	289
HC6	–69	–	–	246	281
HC10	–59	–38	–10	243	268
HC14	–	1; 40; 50	0; 40; 65	216	272
HC16	–	13; 61	10; 46; 64	233	270
T _g – glass transition, T _c – crystallization temperature, T _m – melting point, T _{onset5%} – temperature at which 5% mass loss occurs, T _{onset50%} – temperature at which 50% mass loss occurs					

3.2 Electrochemical experiments

The influence of the protic ionic liquids additives with different substituent length on the electrochemical properties of the lead-calcium-tin alloy for the positive current collector was inspected. The measurements were carried out on one reference electrolyte and five modified ones.

The measurements of the electrochemical stability of the electrolyte showed that protic ionic liquids with bisulfate anion affect the discussed system significantly. Addition of 5 mg cm^{-3} of ILs caused an elongation of the potential window of the sulfuric acid solution on the lead alloy electrode. The relevance of this observation is that the greater the substituent length, the longer it takes until the hydrogen evolution process starts, hence, the wider stability range of the electrolyte. The observed effect of broadening of the electrochemical window of the electrolyte on the lead-alloy electrodes was also reported in the presence of other hydrogen sulfate ionic liquids than the ones presented in this study [26]. It can be assumed that the length of the side chain plays a crucial role in impeding the hydrogen evolution reaction. Moreover, a similar effect referring to the hydrogen evolution reaction was observed not only in case of ammonium but also imidazolium cation [18]. There was no substantial change in the potential of the oxygen evolution. Moreover, there were oxidation and reduction peaks around -1.0 V vs. $\text{Hg}|\text{Hg}_2\text{SO}_4$, which refer to the oxidation and reduction of the lead in the alloy. It can be noticed that their location on the curves is similar in every electrolyte, therefore there is no visible alteration of this process in terms of its potential and intensity (peak current density).

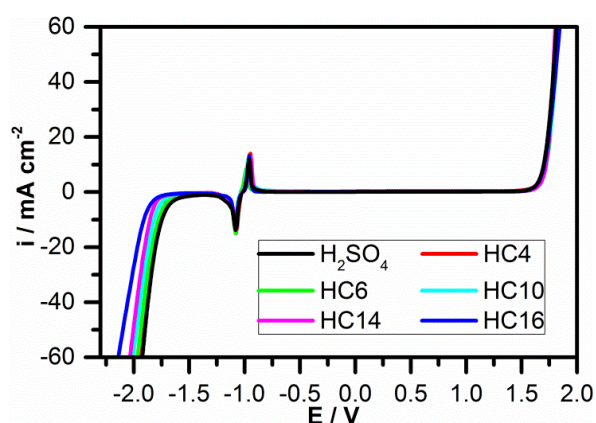


Figure 1. Electrochemical window of the reference and modified electrolytes, using linear sweep voltammetry at scan rate 10 mV s^{-1} , potential measured vs. $\text{Hg}|\text{Hg}_2\text{SO}_4$ reference electrode.

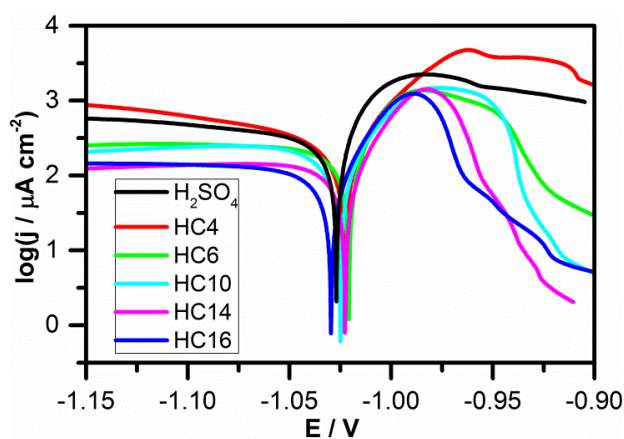


Figure 2. Tafel plots of the examined electrochemical systems, experiment carried out at a scan rate of 0.2 mV s^{-1} within the potential range of $\pm 180 \text{ mV}$ vs. open circuit potential measured by means of $\text{Hg}|\text{Hg}_2\text{SO}_4$.

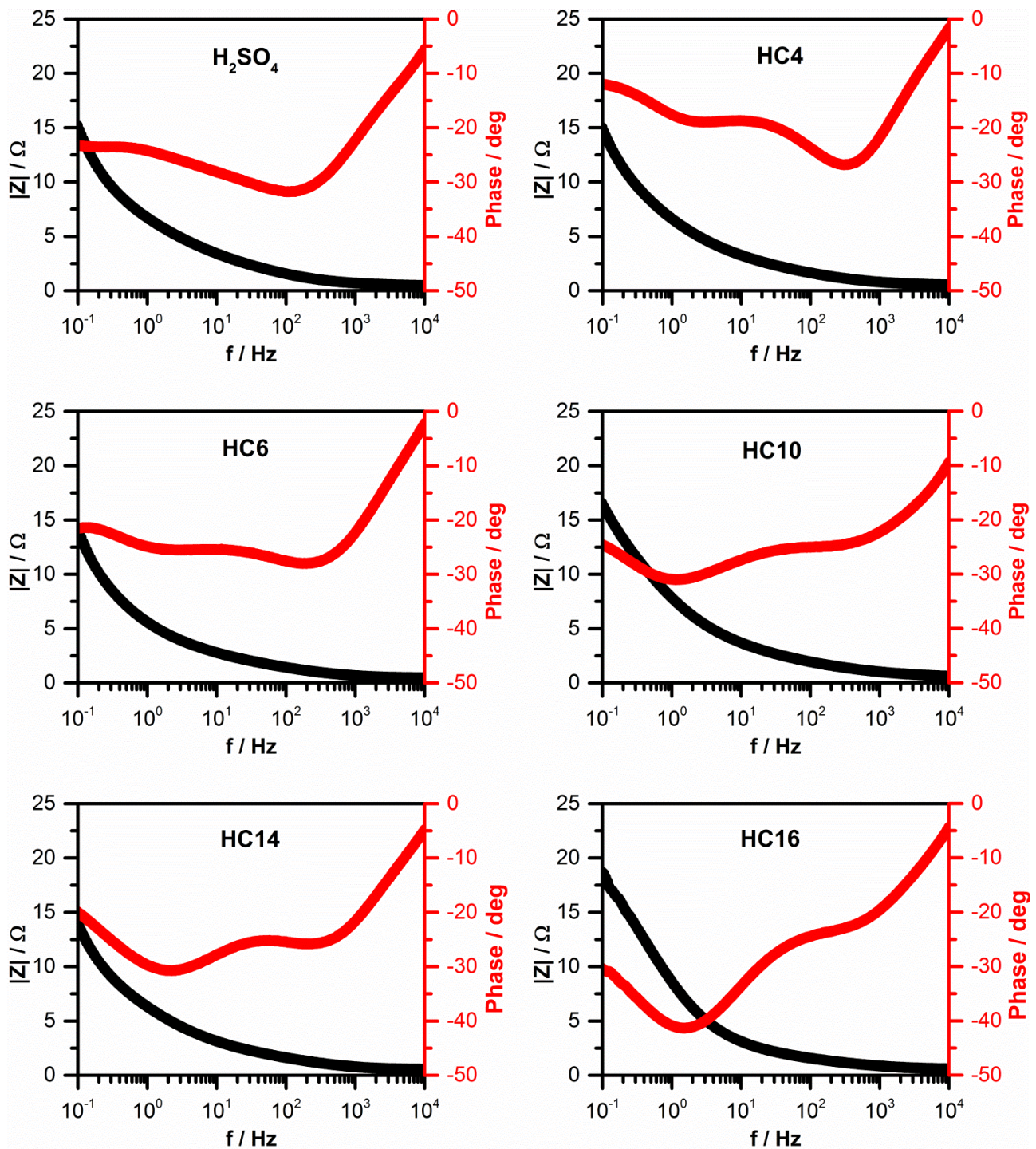


Figure 3. Bode plots of the examined electrochemical systems, experiment carried out at open circuit potential within frequency range from 50 mHz to 10 kHz, overall number of points 200, sinus amplitude $V_{\text{rms}} \pm 7$ mV.

Corrosion potential and corrosion current density were evaluated based on the slope in the Tafel plots, which were obtained using polarization curves. EC-Lab[®] software was employed to calculate the values of the corrosion parameters by means of tangent fitting (Tafel fit). Figure 2 (Fig.2) depicts Tafel plots which characterize the lead alloy in the six used electrolytes. It can be seen that the

corrosion potentials stand at the approximate values in every case, therefore there was no change of this parameter both towards the noble metals and in the opposite direction.

The average value of the corrosion potential of the lead alloy reaches -1025 mV. However, some differences in the values of the corrosion current densities can be observed. In general, the greater the corrosion current, the faster the corrosion rate of the material. It can be noted that the corrosion current density decreased significantly with the length of the substituent, which indicates the deterring of the corrosion rate in the system. Thus, the most beneficial effect was obtained for HC14 and HC16 ionic liquids in the electrolyte. Cathodic and anodic branches of the current-potential curves allowed to calculate Tafel slopes, which depend on e.g. the kinetic of reaction. Values of the above-mentioned parameters were calculated using EC-Lab[®] software based on the potential range of the branch divided by ratio of difference of logarithms of the current axis (decade). Anodic slope β_a is lower than the cathodic one β_c . It could be ascribed to the oxidation process of the main component of the alloy, namely lead, at a potential value of approx. -1.0 V. Furthermore, the trend of the measured values corresponds with the corrosion current density, namely they decrease in the presence of the additive with longer alkyl substituent. Lower Tafel slope at lower current density seems to be a standard electrochemical behavior, observed for other reactions as well [27]. In the undertaken experiment, it is likely connected with forming of the more coherent and stable layer at the surface of the electrode. On the other hand, since there is a long flat branch on the cathodic side, the values of cathodic slopes are higher. It can be stated that polarization resistance increased, when an additional layer forms on the surface of the material. Therefore, the thicker this layer, the greater its value. It can be seen (Table 3) that the lower the corrosion current density, the higher the polarization resistance. Polarization resistance was evaluated basing on the impedance spectroscopy with EC-Lab[®] software. Bode plots depicted below (Fig.3) show that the first time constant and the phase angle increased proportionally to the side chain length in the molecule of the ionic liquid. In these cases, the phase angle varied from -20° for HC4 to -40° for HC16. Therefore, there is a confirmation of the previously made observation that higher corrosion inhibition can be achieved by a small amount of the additive with longer substituent.

Calculated average values and their error ranges are given in the table below (Table 3).

Table 3. Polarization resistance, corrosion potential and corrosion current densities evaluated from EIS and Tafel plots for lead alloy in six electrolytes.

Parameter	Electrolyte					
	Reference solution	HC4	HC6	HC10	HC14	HC16
E_{corr} (LSV), mV	-1026.9 ± 2.4	-1022.8 ± 0.5	-1020.6 ± 0.7	-1024.9 ± 0.1	-1022.6 ± 0.2	-1027.3 ± 0.1
i_{corr} (LSV), $\mu\text{A cm}^{-2}$	251.2 ± 19.8	228.5 ± 23.5	174.1 ± 35.1	132.8 ± 30.7	100.6 ± 25.3	85.4 ± 13.7
β_a , mV dec ⁻¹	38 ± 6	44 ± 8	33 ± 8	29 ± 2	26 ± 5	24 ± 3
β_c , mV dec ⁻¹	200 ± 11	166 ± 17	190 ± 25	172 ± 19	146 ± 12	178 ± 9
R_p (CM), $\Omega \text{ cm}^2$	1.6 ± 0.1	1.7 ± 0.1	4.2 ± 1.0	5.9 ± 0.1	9.9 ± 0.4	15.2 ± 1.7

The possible explanation of such behavior could be forming of a thin organic layer of adsorbed ionic liquids at the surface of the electrode which inhibits the corrosion rate without having adverse influence on the reactions in the system.

4. CONCLUSIONS

The performed experiments enabled to observe the influence of the substituent length in the protic quaternary ammonium ionic liquids on the electrochemical properties of the PbCaSn|H₂SO₄ system. The discussed properties, electrochemical stability of the electrolyte and corrosion behavior of the industrial-grade lead alloy for lead-acid batteries in the modified environment, exhibited relevant changes due to the presence of 5 mg cm⁻³ of the additive in the medium. It can be seen that hydrogen evolution process occurred at more negative potential after the introduction of ionic liquid to the 37 wt.% sulfuric acid solution, thus resulting in a substantial broadening of the electrochemical window of the electrolyte. The strongest effect was observed for the HC16 ionic liquid (side chain with 16 carbon atoms). This observation can indicate that longer substituent positively influenced the system. Moreover, there is no new side reaction which would occur on the surface of the alloy electrode. The implemented ionic liquids induced a change of the corrosion parameters as well. The fundamental conclusion of the experiment would be that the electrochemical behavior of the system improves with the length of the substituent. However, it has to be revised and optimized for the application in the lead-acid battery since there are other factors which play a crucial role in overall usefulness of the additive (e.g. foaming).

ACKNOWLEDGEMENTS

The authors would like to gratefully acknowledge the financial support from the National Centre of Research and Development of Poland, grant No PBS3/A5/43/2015.

References

1. P. Ruetschi, *J. Power Sources*, 127 (2004) 33.
2. G. Lota, M. Baraniak, A. Gabryelczyk, K. Kopczyński, B. Łęgosz, J. Pernak, E. Jankowska, W. Majchrzycki and W. Rzesutek, *Przem. Chem.*, 96 (2017) 1208.
3. M. Dimitrov, D. Pavlov, T. Rogachev, M. Matrakova and L. Bogdanova, *J. Power Sources*, 140 (2005) 168.
4. D. Pavlov, *Lead-acid Batteries. Science and Technology*, Elsevier (2011) Amsterdam, Netherlands.
5. T. Omae, S. Osumi, K. Takahashi and M. Tsubota, *J. Power Sources*, 65 (1997) 65.
6. G. Zhong, W. Su, D. Chen, J. Xiang, X. Wu and J. Chen, An influence study of hydrogen evolution characteristics on the negative strap corrosion of lead-acid battery, International Conference on Energy, Materials and Manufacturing Engineering, Kuala Lumpur, Malaysia, 2015, 02001.
7. C. Verma, E. E. Ebenso and M. A. Quraishi, *J. Mol. Liq.*, 233 (2017) 403.
8. M. Finšgar and J. Jacksson, *Corrosion Sci.*, 86 (2014) 17.

9. C. G. Dariva and A. F. Galio (2014). Corrosion Inhibitors – Principles, Mechanisms and Applications, Developments in Corrosion Protection, M. Aliofkhazraei (Ed.), InTech, DOI: 10.5772/57255.
10. K. Park, S. Yu, C. Lee and H. Lee, *J. Power Sources*, 296 (2015) 197.
11. R. T. Loto, C. A. Loto and A. P. I. Popoola, *J. Mater. Environ. Sci.*, 3 (2012) 885.
12. Q. B. Zhang and Y. X. Hua, *Electrochim. Acta*, 54 (2009) 1881.
13. Q. B. Zhang and Y. X. Hua, *Mater. Chem. Phys.*, 119 (2010) 57.
14. Q. B. Zhang and Y. X. Hua, Ionic Liquids as Electrodeposition Additives and Corrosion Inhibitors, Progress and Developments in Ionic Liquids, Scott Handy (Ed.), InTech (2017) DOI: 10.5772/65807.
15. Y. Sasikumar, A. S. Adekunle, L. O. Olasunkanmi, I. Bahadur, R. Baskar, M. M. Kabanda, I. B. Obot and E. E. Ebenso, *J. Mol. Liq.*, 211 (2015) 105.
16. R. S. Kühnel, M. Lübke, M. Winter, S. Passerini and A. Balducci, *J. Power Sources*, 214 (2012) 178.
17. A. Gabryelczyk, K. Kopczyński, M. Baraniak, B. Łęgosz, F. Walkiewicz, J. Pernak, E. Jankowska, W. Majchrzycki, P. Kędzior and G. Lota, *J. Solid State Electrochem.*, DOI: 10.1007/s10008-017-3817-7.
18. B. Rezaei, S. Mallakpour and M. Taki, *J. Power Sources*, 187 (2009) 605.
19. K. Kopczyński, M. Baraniak, J. Pernak, R. Giszter, M. Fryder and G. Lota, *Chemik*, 70 (2016) 509.
20. M. Stasiewicz, K. Materna, D. Pęziak-Kowalska and G. Lota, *Int. J. Electrochem. Sci.*, 10 (2015) 10513.
21. J. S. Lee, K. Sakaushi, M. Antonietti and J. Yuan, *RSC Adv.*, 5 (2015) 85517.
22. Y. Guo, B. Xu, Y. Liu, W. Yang, X. Yin, Y. Chen, J. Le and Z. Chen, *J. Indust. Eng. Chem.*, 56 (2017) 234.
23. H. Ohno, *Electrochemical Aspects of Ionic Liquids*, Wiley (2011) Tokyo, Japan.
24. A. A. J. Torriero (ed.), *Electrochemistry in Ionic Liquids vol. 1. Fundamentals*, Springer (2015) Cham, Switzerland.
25. S. Zhang, N. Sun, X. He, X. Lu and X. Zhang, *J. Phys. Chem. Ref. Data*, 35 (2006) 1475.
26. B. Rezaei, A. A. Ensafi, A. R. T. Jahromi, *Ionics*, 18 (2012) 109.
27. K. Kinoshita, *Electrochemical Oxygen Technology*, Wiley (1992) NewYork, USA.